

## Land Cover Segmentation of Multispectral Images Using U-Net and DeeplabV3+ Architecture

Herlawati<sup>1</sup>, Rahmadya Trias Handayanto<sup>2</sup>

<sup>1</sup>Informatics, Faculty of Computer Science, Universitas Bhayangkara Jakarta Raya, Indonesia

<sup>2</sup>Computer Engineering, Faculty of Engineering, Universitas Islam 45, Indonesia

E-mail: <sup>1</sup>[herlawati@ubharajaya.ac.id](mailto:herlawati@ubharajaya.ac.id), <sup>2</sup>[rahmadya.trias@gmail.com](mailto:rahmadya.trias@gmail.com)

### Abstract

The application of Deep Learning has now extended to various fields, including land cover classification. Land cover classification is highly beneficial for urban planning. However, the current methods heavily rely on statistical-based applications, and generating land cover classifications requires advanced skills due to their manual nature. It takes several hours to produce a classification for a province-level area. Therefore, this research proposes the application of semantic segmentation using Deep Learning techniques, specifically U-Net and DeepLabV3+, to achieve fast land cover segmentation. This research utilizes two scenarios, namely scenario 1 with three land classes, including urban, vegetation, and water, and scenario 2 with five land classes, including agriculture, wetland, urban, forest, and water. Experimental results demonstrate that DeepLabV3+ outperforms U-Net in terms of both speed and accuracy. As a test case, Landsat satellite images were used for the Karawang and Bekasi Regency areas.

**Keywords:** *deeplabv3+, landsat satellite, semantic segmentation, u-net, multispectral.*

### 1. Introduction

Computer Vision is a branch of computer science that finds applications in various fields such as medicine, transportation, remote sensing, and more. One of the benefits it provides is the speed of processing and high accuracy achieved in recent times. However, one area that still lacks widespread adoption of Deep Learning is Remote Sensing, particularly in Land Cover classification. This is despite certain tasks requiring a significant amount of data, such as land use change prediction, where Land Cover classifications for specific periods are crucial. If generating a single classification map already consumes considerable time, the challenge becomes greater when multiple data sets are required for different periods (typically annual data). Computer Vision encompasses various tasks such as classification, object detection, segmentation, image restoration, and more. Land Cover classification falls under the segmentation category, where each pixel represents a specific land cover type [1]–[4].

Satellite imagery is easily accessible nowadays, for example, through the official USGS website, which provides Landsat satellite data. Users can

select specific dates within a given year and choose multispectral images, where multiple bands are available for specific sensors, such as red, green, blue, infrared, and more. With a larger number of bands, it is expected to achieve better accuracy in land cover classification, including categories such as buildings, vegetation, water bodies, wetlands, and other land cover types.

Previous researchers have applied U-Net for land use/cover classification using six Landsat bands, namely bands 2 to 7. The accuracy achieved was quite good in classifying several land use/cover categories. However, the proposed method requires the use of drones or Unmanned Aerial Vehicles (UAVs), which can be costly [5].

U-Net, which is based on Convolutional Neural Networks (CNNs), has certain limitations, such as the vanishing/exploding gradient problem [6], [7]. As a result, some researchers have replaced it with ResNet for the encoder and decoder sides. Additionally, by incorporating the Atrous Spatial Pyramid Pooling (ASPP), a DeepLabV3+ model is believed to be able to handle large-scale image classification tasks [8]. This is significant considering that U-Net is primarily applied to

small-scale medical images [9], [10]. Both U-Net [11]–[14] and DeepLabV3+ [15]–[18] have undergone numerous modifications to improve performance and adapt to hardware conditions with limited computational resources [19].

Since research utilizing satellite imagery is still relatively scarce [20], and the majority of studies have yet to incorporate multispectral imagery [21], [22], This study modifies the conventional semantic segmentation model, which typically utilizes drone-captured images, to be based on multispectral satellite images. The performance of two well-known methods, i.e., U-Net and DeepLabV3+, will be analyzed considering that both models have specific applications. U-Net is typically used for small-sized medical images, while DeepLabV3+ is commonly employed for large-scale images.

We aim to bridge this gap by utilizing commonly used satellite images in RS-GIS, particularly utilizing the band frequency sensor. The results of this research serve as a benchmark for future research focusing on modified existing methods using satellite images, which have the advantage of capturing wide areas. The rest of the paper is organized as follows. After explaining the data sources and deep learning models used, two prototypes were created to facilitate testing, and their performance was evaluated.

## 2. Materials and Methods

This study used two Deep Learning models as benchmarks to make it easier for RS-GIS practitioners to classify land cover. Tests were carried out in two locations, namely the western region of Karawang and Bekasi district to find out whether it was feasible or not to be implemented in other areas. Data obtained from Landsat satellite imagery provided by USGS was used (<https://earthexplorer.usgs.gov/>), captured on May 11, 2021. The captured area covered a single tile encompassing the JABOTABEK region. As a preliminary processing step, the data needed to be cropped to match the research area, which includes the Karawang and Bekasi Regency regions.

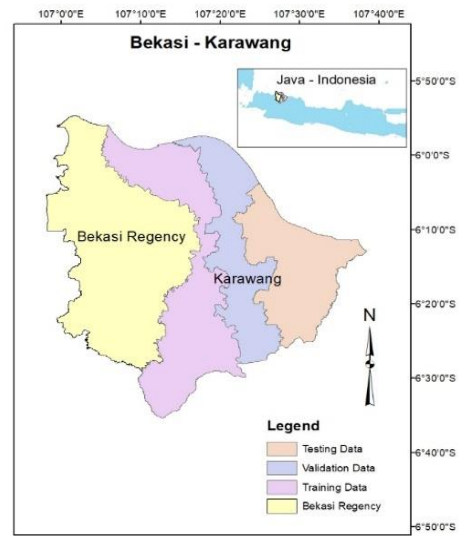


Fig. 1. Training and Testing Areas.

The Karawang region was selected as the training data for the U-Net and DeepLabV3+ models, while the Bekasi Regency was used as the testing location. The Karawang and Bekasi regions are located on the island of Java, Indonesia, with latitude and longitude coordinates are approximately  $6^{\circ}10'$  and  $107^{\circ}20'$ , respectively. Figure 1 illustrates the training, validation, and testing data areas within the research area. The selected segment classes follow the standard land use/cover classification rules, where Landsat falls into category I [23]. Figure 2 shows the preprocessing process for preparing the training data, validation data, and test data for the Karawang region, which has an area of  $1911 \text{ km}^2$ . The same process is performed for the Bekasi district, which has an area of  $1274 \text{ km}^2$  as the testing area. The final process shows the pixel dimensions for Karawang and Bekasi, which are 5,877,336 pixels and 2,577,920 pixels, respectively. To generate a model for the Karawang region, this area is divided into three regions, each for training, validation, and testing data. The sizes of the training, validation, and testing data are 1,439,328 pixels, 1,679,208 pixels, and 2,758,800 pixels, respectively.

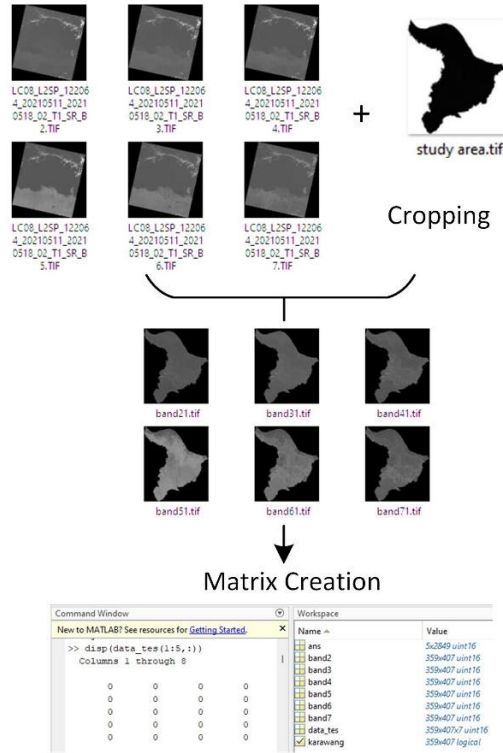


Fig. 2. Preprocessing Satellite Imageries to Dataset

Two scenarios were chosen: scenario one with three classes (urban, vegetation, and water) and scenario two with five classes, including agriculture, wetland, urban, forest, and water. The first scenario with three classes is basic, where most land covers in other tropical areas have those classes. The second scenario divide vegetation into agriculture and forest, as well as the water into water and wetland since the study area uses wetland and water as its land use zones. The ground truth datasets, consisting of classified segments, are used for accuracy calculations. The ground truth is created using TerrSet through the Iterative Self-Organizing Clustering (ISOCCLUS) method, which is then followed by manual reclassification to ensure that the clustering results can differentiate segments according to the scenario.

The MATLAB 2021a version was chosen for the training and evaluation process. MATLAB live script for training refers to the official MATLAB website, i.e., for U-Net as a baseline method which used non-satellite imagery, i.e., RIT-18 dataset with 18 classes [24]. The RIT-18 is high resolution on small area with 18 classes that did not meet the requirement of land use/cover practitioners, e.g., picnic table, buoy, road marking, etc. Therefore, we train with satellite images from scratch. For the DeepLabV3+ model, we utilized the available model library in MATLAB’s Network Designer. To convert image files into MAT files in the form of matrices, a conversion process is required.

Figure 3 illustrates the U-Net model. The small circles in the model represent one convolutional layer/block. The structure of the encoder and decoder forms a shape resembling the letter 'U,' which is why it is named U-Net. The U-Net has fewer layers compared to DeepLabV3+ due to the issues of vanishing and exploding gradients.

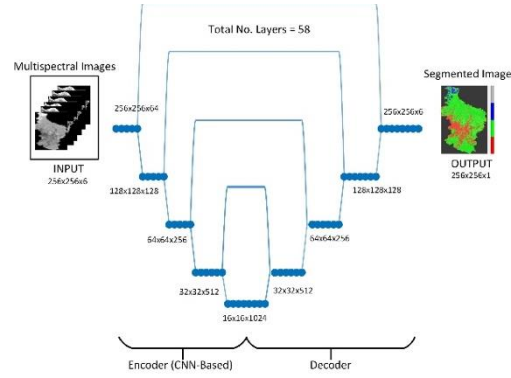


Fig. 3. U-Net Architecture

U-Net utilizes a series of 2D convolution processes with pooling and bias with the following formula:

$$\omega * F(x, y) = \left( \sum_{\delta x=-k_i}^{k_i} \sum_{\delta y=-k_j}^{k_j} \omega(\delta x, \delta y) \cdot F(x + \delta x, y + \delta y) \right) + \omega_{bias} \quad (1)$$

where  $\omega_{bias} \in \mathbb{R}$  is bias of the kernel  $\omega$

The cross-entropy loss function in equation 2 is used to measure how closely the predictions of the U-Net model approximate the true values.

$$L_{CE} = - \sum_{i=1}^n t_i \log(p_i), \text{ for } n \text{ classes} \quad (2)$$

Where  $t_i$  is the true label and  $p_i$  is the SoftMax probability for class- $i$ . The activation functions used include ReLU, Sigmoid, and SoftMax, following equations 3-5.

$$R(z) = \begin{cases} -x, & x < 0 \\ x, & x \geq 0 \end{cases} \quad (3)$$

$$(z) = \frac{1}{1+e^{-z}} \quad (4)$$

$$\text{SoftMax}(z_j) = \frac{e^{z_j}}{\sum_{k=1}^K e^{z_k}} \text{ for } j = 1, \dots, K \quad (5)$$

Both U-Net and DeepLabV3+ (Figure 4) utilize encoder and decoder structures. While U-Net’s encoder and decoder use CNN blocks, DeepLabV3+’s encoder and decoder employ ResNet50 blocks. Additionally, in the bottleneck section of DeepLabV3+, Atrous Spatial Pyramid Pooling (ASPP) is performed to extract features from objects of various sizes. The copy and crop operation in DeepLabV3+ is only applied to specific expansions/contractions, unlike U-Net, which is performed at each expansion/contraction.

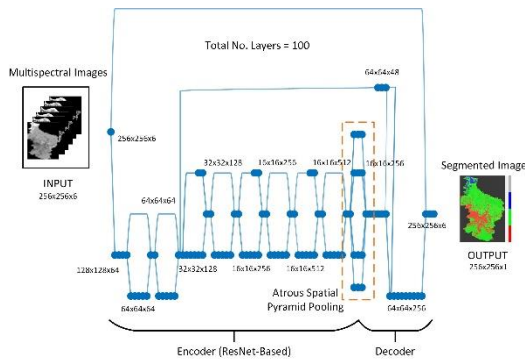


Fig. 4. DeepLabV3+ Architecture

Table 1 shows the parameters and hyperparameters of U-Net and DeepLabV3+. Here, hyperparameters are set the same to produce a fair comparison. It appears that U-Net has a larger number of parameters and model size compared to DeepLabV3+ despite DeepLabV3+ having nearly twice the number of layers as U-Net.

Table 1. Parameters and Hyperparameters of U-Net and DeepLabV3+

Network Info		U-Net	DeepLabV3+
Parameters	# of layer	58 layers	100 layers
	Size	110.22 Mbyte	58.39 Mbyte
	# of params	31.03 M	20.62 M
Hyperparameters	Max Epoch	2 (2000 iteration)	
	Initial learning rate	0.05	
	Minibatch size	16	
	L2-regularization	0.0001	
	Training option	stochastic gradient descent with momentum (SGDM)	
gradient threshold	0.05		

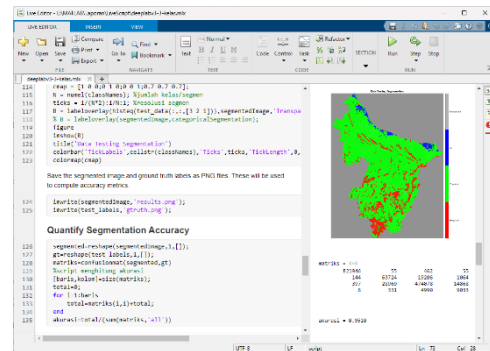
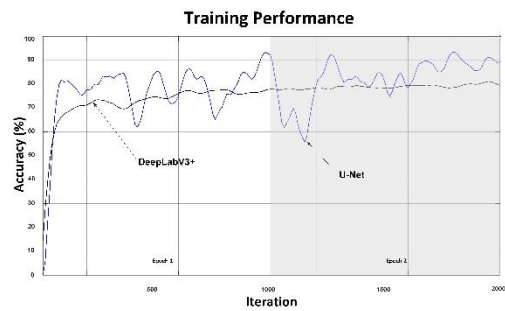
Accuracy is calculated based on the confusion matrix, which compares the predictions of U-Net and DeepLabV3+ with the actual values (Ground Truth). Additionally, the processing speed in making predictions is also recorded to assess the performance of the land cover segmentation. To ensure a fair comparison, the number of epochs is kept the same for both U-Net and DeepLabV3+ during training, which is 2 epochs with 2000 iterations.

### 3. Result and Discussion

The Graphic User Interface (GUI) using the MATLAB 2021a programming language is created to facilitate the testing process. It consists of U-Net and DeepLabV3+ for segmenting scenario 1 with three-segment land cover classes and scenario 2 with five-segment land cover classes. With

compilation, the created GUI can be executed on other computers without having MATLAB installed.

The training process takes several hours for each model. Figure 5 illustrates the training performance, with U-Net exhibiting high fluctuations. The training was executed using the NVIDIA GeForce MX130 Graphic Processing Unit (GPU). To achieve higher accuracy levels, hardware with longer training time (tens or even hundreds of epochs) is required. However, for comparing the feasibility of the two methods in the segmentation process, the used hardware is still suitable. In addition, from the training process graph, it is noticeable that the accuracy improvement starts to slow down as early as the



second epoch.

Fig. 4. Training Performance and Testing-Result Illustration in MATLAB live script

The trained model, in the form of MAT files, is then used for land cover segmentation prediction in another area that was not involved in the training process. The three classes scenario is basic, where vegetation, urban, and water prediction shows 94% accuracy for U-Net and 95% accuracy for DeepLabV3+. Table 2 and Figure 5 show the metrics of model performance based on equation (6) – (9). Water appears to be the class with the lowest accuracy, while agriculture has the highest accuracy.

$$precision = \frac{TP}{TP+FP} \quad (6)$$

$$recall = \frac{TP}{TP+FN} \quad (7)$$

$$F1 - score = 2 \times \frac{precision \times recall}{precision+recall} \quad (8)$$

$$IoU = \frac{\text{object ndetected box}}{\text{object vdetected box}} \quad (9)$$

**Table 2.** Testing Result of DeepLabV3+ and U-Net (in brackets)

Class	Precision	Recall	F1-Score	IoU
Agri	88.26 (83.83)	84.08 (84.21)	86.12 (84.02)	75.63 (72.44)
Wetland	69.96 (88.29)	74.70 (62.50)	72.25 (73.19)	56.56 (57.71)
Urban	88.41 (76.21)	54.72 (57.24)	67.60 (65.38)	51.06 (48.56)
Forest	54.45 (56.78)	74.14 (70.07)	62.79 (62.73)	45.76 (45.70)
Water	53.87 (19.77)	59.35 (85.70)	56.48 (32.13)	39.35 (19.14)
Accuracy	88.313 (87.654)			
mIoU	53.67 (48.71)			

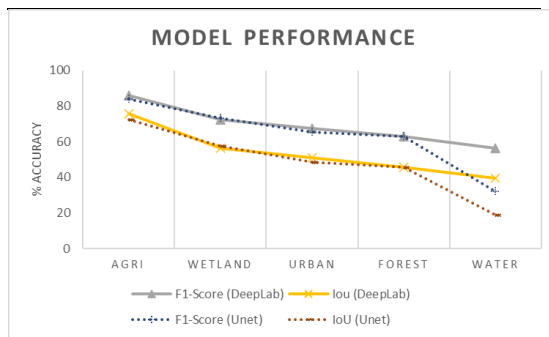


**Fig. 5.** Accuracy Comparison of DeepLabV3+and UNet

The testing was conducted using test data from Karawang Regency (the right part of Karawang as shown in Fig1), both for U-Net and DeepLabV3+. DeepLabV3+ showed superiority in terms of accuracy and speed. Figure 6 shows the accuracy of U-Net and DeepLabV3+ to be 87.65% and 88.31%, respectively. The speed of DeepLabV3+ was less than 1 minute, while U-Net took around 6 minutes.

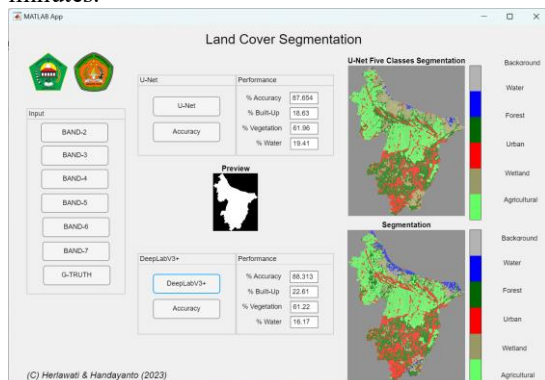


**Fig. 6.** Segmentation of U-Net and DeepLabV3+ Using Testing Dataset

Another area, i.e., Bekasi Regency, was used for testing as shown in Figure 1. This area is

adjacent to Karawang Regency. Two prototypes, one for U-Net and one for DeepLabV3+, are prepared to facilitate model testing. This testing aims to determine the suitability of the model for implementation in other regions besides Karawang.

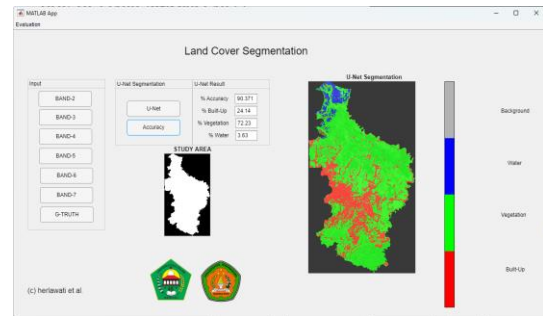


**Fig. 7.** U-Net Segmentation for Three Class Segments

Figure 7 shows the segmentation results using U-Net. By inputting the cropped satellite images from band 2 to band 6 within the study area, U-Net achieves a land cover segmentation accuracy of 90.37% in just 6 minutes. The percentages of Built-Up/Urban, Vegetation, and Water are 24.14%, 72.23%, and 3.63%, respectively.

Meanwhile, DeepLabV3+ (Fig. 8) achieves a slightly higher segmentation accuracy of 90.98%. However, it is important to note that it also exhibits improved speed, completing the segmentation in less than one minute.

One thing to note is the model complexity, where U-Net, with almost half the number of layers compared to DeepLabV3+, only lags by 0.61% in terms of performance.

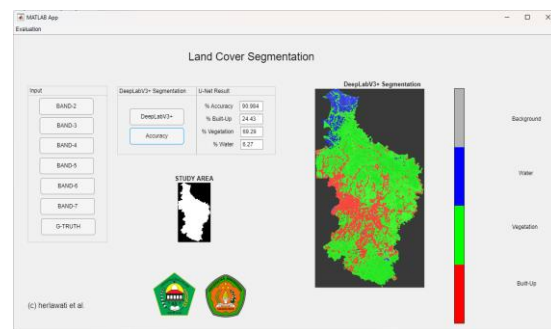


**Fig. 8.** DeepLabV3+ Segmentation for Three Class Segments

Overall, DeepLabV3+ slightly outperforms its predecessor, U-Net. Table 3 provides a comparison between U-Net and DeepLabV3+ in terms of accuracy, processing speed, model complexity, and training characteristics for scenario 1 for three classes. The percentages of Built-Up/Urban, Vegetation, and Water are 24.43%, 69.29%, and 6.27%, respectively. The

illustration of the segmentation process can be seen in the following link: <https://youtu.be/097qXm3qvWo>.

**Table 3.** Comparison between U-Net and DeepLabV3+ for Three Classes of Segment

No.	Aspects Compared	U-Net	DeepLabV3+
1	Accuracy	90.37%	90.98%
2	Inference Time	6 minutes	1 minutes
3	Model Complexity	58 layers	100 layers
4	Training Characteristics	Fluctuating	Stable

Scenario 2 with five classes (agriculture, wetland, urban, forest, and water) shows a decrease in accuracy. This is expected to be due to the difficulty of the model in distinguishing similar classes, such as agriculture and forest, or wetland and water. Figure 9 and Table 3 show the performance of U-Net and DeepLabV3+ in the segmentation process.

**Table 3.** Comparison between U-Net and DeepLabV3+ for Five classes of Segment

No.	Aspects Compared	U-Net	DeepLabV3+
1	Accuracy	68.88%	71.73%
2	Inference Time	6 minutes	1 minutes
3	Model Complexity	58 layers	100 layers
4	Training Characteristics	Fluctuating	Stable

The calculation results show that scenario 1 with three-segment classes demonstrates good performance when applied to other regions. These three classes, namely urban, vegetation, and water, represent the most common land cover types in Indonesia. Some land cover types, such as wetlands, may not be present in other areas. The testing indicates that scenario 1 can be used for other regions in Indonesia.

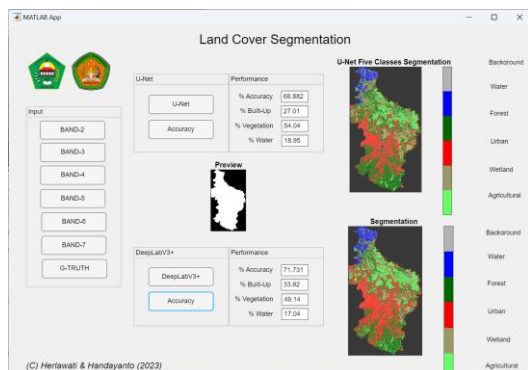


**Fig. 9.** Performance of U-Net and DeepLabV3+ for Five Classes Segmentation

Referring to the Cross-Industry Standard Process for Data Mining (CRISP-DM) [25], [26], another important aspect is "deployment," where users should benefit from the developed model. In addition to generating segmented images on a Graphic User Interface (GUI), a Figure window was generated as well.

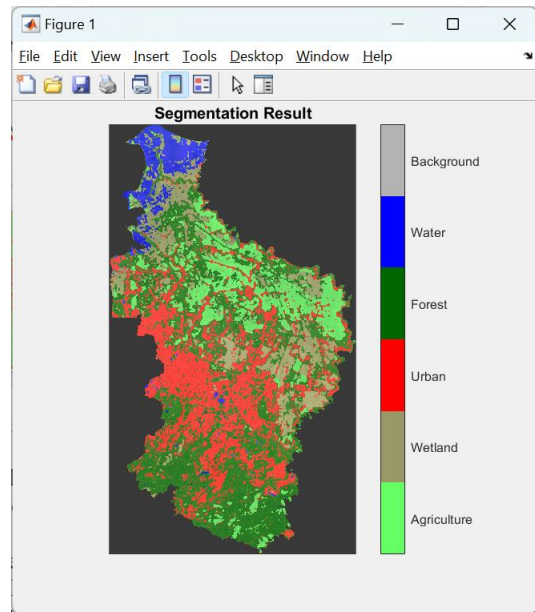


**Fig. 10.** Figure Window for Saving the Result

Figure 10 shows the window that can save the classification results in TIFF format. This is crucial, considering that the segmentation process is based solely on image data, and further processing is required by Remote Sensing and Geographic Information Systems (RS-GIS) practitioners through digitization and georeferencing functions.

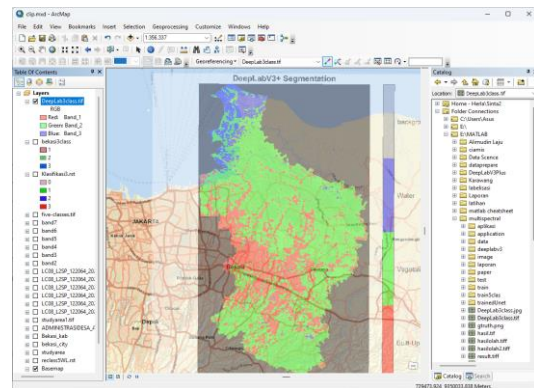


**Fig. 11.** The Segmentation result runs on ArcMap.

Users can then open the TIFF file to display it in GIS Tools, such as ArcMap 10.7, as shown in Figure 11 after performing georeferencing to

obtain the appropriate coordinates and projection as well as adding a base map. With the base map, users can visualize the real conditions, both in terms of location (roads, cities, etc.) and satellite imagery if a satellite view base map is selected.

The prototype used is desktop-based, which is commonly employed by vertical applications available in the market, particularly for geospatial analysis such as TerrSet, eCognition, ArcGIS, and others. Additionally, the segmentation process involves data with large-sized pixels (at the city/district level), which can be resource-intensive to run on web-based or mobile applications.

The trained models, both U-Net and DeepLabV3+, can be directly used for other regions with their respective accuracy levels for scenario 1 and scenario 2, which can be seen in Table 1 and Table 2. However, for regions outside of Indonesia, retraining is necessary due to different characteristics such as deserts, snow, and other land cover classes.

#### 4. Conclusion

The use of deep learning in land cover segmentation accelerates the segmentation process from hours to minutes. Additionally, it eliminates the need for specialized skills in classifying land cover types from segmentation using conventional applications such as TerrSet, eCognition, ENVI, and similar tools. By inputting bands 2 to 7 of the cropped satellite imagery within the study area, the model can produce a segmented land cover map. DeepLabV3+ slightly outperforms U-Net in terms of performance (accuracy and speed), but U-Net has a simpler structure. Future research should focus on developing new models or hybrids that leverage the strengths of various deep learning models such as MobileNet, Inception, Xception, and others.

#### References

- [1] H. Wu, Q. Liu, and X. Liu, "A review on deep learning approaches to image classification and object segmentation," *Computers, Materials and Continua*, vol. 60, no. 2, pp. 575–597, 2019.
- [2] L. Khelifi and M. Mignotte, "Deep Learning for Change Detection in Remote Sensing Images: Comprehensive Review and Meta-Analysis," *IEEE Access*, vol. 8, no. Cd, pp. 126385–126400, 2020.
- [3] T. Hoeser and C. Kuenzer, "Object detection and image segmentation with deep learning on Earth observation data: A review-part I: Evolution and recent trends," *Remote Sensing*, vol. 12, no. 10, 2020.
- [4] N. Audebert, B. Le Saux, and S. Lefevre, "Deep learning for classification of hyperspectral data: A comparative review," *IEEE Geoscience and Remote Sensing Magazine*, vol. 7, no. 2, pp. 159–173, 2019.
- [5] R. Kemker, C. Salvaggio, and C. Kanan, "Algorithms for semantic segmentation of multispectral remote sensing imagery using deep learning," *ISPRS Journal of Photogrammetry and Remote Sensing*, vol. 145, no. March, pp. 60–77, 2018.
- [6] A. Shah, E. Kadam, H. Shah, S. Shinde, and S. Shingade, "Deep residual networks with exponential linear unit," *ACM International Conference Proceeding Series*, vol. 21–24–Sept, pp. 59–65, 2016.
- [7] M. Roodschild, J. Gotay Sardiñas, and A. Will, "A new approach for the vanishing gradient problem on sigmoid activation," *Progress in Artificial Intelligence*, vol. 9, no. 4, pp. 351–360, 2020.
- [8] L.-C. Chen, Y. Zhu, G. Papandreou, F. Schrof, and H. Adam, *Encoder-Decoder with Atrous Separable Convolution for Semantic*. Switzerland: Springer International Publishing, 2018.
- [9] A. A. Pravitasari *et al.*, "UNet-VGG16 with transfer learning for MRI-based brain tumor segmentation," *Telkomnika (Telecommunication Computing Electronics and Control)*, vol. 18, no. 3, pp. 1310–1318, 2020.
- [10] I. Z. Matovinovic, S. Loncaric, J. Lo, M. Heisler, and M. Sarunic, "Transfer learning with U-net type model for automatic segmentation of three retinal layers in optical coherence tomography images," *International Symposium on Image and Signal Processing and Analysis, ISPA*, vol. 2019–Sept, pp. 49–53, 2019.
- [11] P. Kumar, P. Nagar, C. Arora, and A. Gupta, "U-Net: Fully Convolutional Neural Network Based Automated Brain Tissue Segmentation Tool," *Proceedings - International Conference on Image Processing, ICIP*, pp. 3503–3507, 2018.
- [12] J. Wang, P. Lv, H. Wang, and C. Shi, "SAR-U-Net: Squeeze-and-excitation block and atrous spatial pyramid pooling based residual U-Net for automatic liver segmentation in Computed Tomography," *Computer Methods and Programs in Biomedicine*, vol. 208, pp. 1–25, 2021.
- [13] S. Cai, Y. Tian, H. Lui, H. Zeng, Y. Wu, and G. Chen, "Dense-unet: A novel multiphoton in vivo cellular image segmentation model based on a convolutional neural network," *Quantitative Imaging in Medicine and Surgery*, vol. 10, no. 6, pp. 1275–1285, 2020.
- [14] O. Oktay *et al.*, "Attention U-Net: Learning Where to Look for the Pancreas," no. Midl, 2018.
- [15] M. Wieland, S. Martinis, R. Kiefl, and V. Gstaiger, "Semantic segmentation of water bodies in very high-resolution satellite and aerial images," *Remote Sensing of Environment*, vol. 287, 2023.
- [16] T. Shi, Z. Guo, C. Li, X. Lan, X. Gao, and X. Yan, "Improvement of deep learning Method for water body segmentation of remote sensing images based on attention modules," *Earth Science Informatics*, 2023.
- [17] K. Zheng, H. Wang, F. Qin, C. Miao, and Z. Han, "An Improved Land Use Classification Method Based on DeepLab V3+ Under GauGAN Data Enhancement," *IEEE Journal of Selected Topics in Applied Earth Observations and Remote Sensing*, vol. 16, pp. 5526–5537, 2023.
- [18] Y. Yuan and Y. Tian, "Semantic Segmentation Algorithm of Underwater Image Based on Improved DeepLab v3+," in *Proceedings of SPIE - The International Society for Optical Engineering*, 2023, vol. 12604.
- [19] P. Wang *et al.*, "Environment Understanding Algorithm for Substation Inspection Robot Based on Improved DeepLab V3+," *Journal of Imaging*, vol. 8, no. 10, 2022.
- [20] J. Bai *et al.*, "Hyperspectral Image Classification Based on Multibranch Attention Transformer Networks," *IEEE Transactions on Geoscience and Remote Sensing*, vol. 60, 2022.
- [21] P. Helber, B. Bischke, A. Dengel, and D. Borth, "Eurosat: A novel dataset and deep learning benchmark for land use and land cover

- classification,” *IEEE Journal of Selected Topics in Applied Earth Observations and Remote Sensing*, vol. 12, no. 7, pp. 2217–2226, 2019.
- [22] S. Desai and D. Ghose, “Active Learning for Improved Semi-Supervised Semantic Segmentation in Satellite Images,” in *Proceedings - 2022 IEEE/CVF Winter Conference on Applications of Computer Vision, WACV 2022*, 2022, pp. 1485–1495.
- [23] C. P. Giri, *Remote Sensing of Land Use and Land Cover*. United States of America: CRC Press, 2012.
- [24] Mathworks, “Semantic Segmentation of Multispectral Images Using Deep Learning,” 2023. [Online]. Available: <https://www.mathworks.com/help/images/multispectral-semantic-segmentation-using-deep-learning.html>. [Accessed: 13-Jan-2023].
- [25] IBM, “IBM SPSS Modeler CRISP-DM Guide,” 2023. [Online]. Available: <https://www.ibm.com/docs/en/spss-modeler/18.1.1?topic=spss-modeler-crisp-dm-guide>.
- [26] C. Schröer, F. Kruse, and J. M. Gómez, “A systematic literature review on applying CRISP-DM process model,” *Procedia Computer Science*, vol. 181, no. 2019, pp. 526–534, 2021.